

A Stretchable Yarn Embedded Triboelectric Nanogenerator as Electronic Skin for Biomechanical Energy Harvesting and Multifunctional Pressure Sensing

Kai Dong, Zhiyi Wu, Jianan Deng, Aurelia C. Wang, Haiyang Zou, Chaoyu Chen, Dongmei Hu, Bohong Gu, Baozhong Sun, and Zhong Lin Wang*

Flexible and stretchable physical sensors capable of both energy harvesting and self-powered sensing are vital to the rapid advancements in wearable electronics. Even so, there exist few studies that can integrate energy harvesting and self-powered sensing into a single electronic skin. Here, a stretchable and washable skin-inspired triboelectric nanogenerator (SI-TENG) is developed for both biomechanical energy harvesting and versatile pressure sensing. A planar and designable conductive yarn network constructed from a three-ply-twisted silver-coated nylon yarn is embedded into flexible elastomer, endowing the SI-TENG with desired stretchability, good sensitivity, high detection precision, fast responsivity, and excellent mechanical stability. With a maximum average power density of 230 mW m^{-2} , the SI-TENG is able to light up 170 light-emitting diodes, charge various capacitors, and drive miniature electronic products. As a self-powered multifunctional sensor, the SI-TENG is adopted to monitor human physiological signals, such as arterial pulse and voice vibrations. Furthermore, an intelligent prosthetic hand, a self-powered pedometer/speedometer, a flexible digital keyboard, and a proof-of-concept pressure-sensor array with 8×8 sensing pixels are successively demonstrated to further confirm its versatile application prospects. Based on these merits, the developed SI-TENG has promising applications in wearable powering technology, physiological monitoring, intelligent prostheses, and human-machine interfaces.

our physical world. Motivated by the effort to create an artificial skin with human-like sensory capabilities, the field of electronic skin (e-skin) is attracting a great deal of attention in both commercial development and the research community due to its exciting potential applications in touch-sensor-based technologies,^[1–3] artificial intelligence systems,^[4–7] personal healthcare monitoring,^[8–10] and human-machine interfaces.^[11–13] In order to exhibit the unique properties of human skin, e-skin must conform to cover dynamic and irregular surfaces and withstand a variety of repeated and prolonged mechanical stimuli, such as pressure, strain, and flexion.^[14,15] Additionally, as a multifunctional and durable sensor, it must satisfy the requirements of high stretchability, high sensitivity, wide sensing range, and fast responsivity.^[16,17]

Until now, various flexible and stretchable physical sensors as e-skins that measure and quantify electrical signals generated from human activity have been achieved based on different sensing mechanisms, in particular piezoelectricity,^[6,18,19] capacitance,^[20,21] and piezoresistivity.^[1,10,22–24]

Depending on the active materials and device structure, each of these sensing mechanisms has its own characteristics. Piezoelectric-based sensors rely on the piezoelectric

Mimicry of the basic characteristics of human skin via functional electronic devices is an important step in developing intelligent technology that can easily integrate with

Dr. K. Dong, Dr. Z. Wu, Dr. J. Deng, A. C. Wang, H. Zou, C. Chen, Prof. Z. L. Wang
School of Material Science and Engineering
Georgia Institute of Technology
Atlanta, GA 30332-0245, USA
E-mail: zhong.wang@mse.gatech.edu

Dr. K. Dong, Prof. B. Gu, Prof. B. Sun
College of Textiles
Key Laboratory of High Performance Fibers & Products
Ministry of Education
Donghua University
Shanghai 201020, P. R. China

 The ORCID identification number(s) for the author(s) of this article can be found under <https://doi.org/10.1002/adma.201804944>.

Dr. D. Hu
Key Lab of Nano-Devices and Applications
Suzhou Institute of Nano-Tech and Nano-Bionics
Chinese Academy of Sciences
Suzhou, Jiangsu 215123, P. R. China

Prof. Z. L. Wang
Beijing Institute of Nanoenergy and Nanosystems
Chinese Academy of Sciences
Beijing 100083, P. R. China

Prof. Z. L. Wang
School of Nanoscience and Technology
University of Chinese Academy of Sciences
Beijing 100049, P. R. China

DOI: 10.1002/adma.201804944

effect that enables mechanical stimulations to be converted into an electric signal. Piezoelectric sensors demonstrate ultrafast response, high sensitivity, and low power consumption. However, they are limited in flexibility, stretchability, and detection in the low-pressure range. Therefore, the piezoelectric sensors lack the stability to wrap on curved objects or the human body. Piezoresistive sensors rely on the changes of electrical resistance in response to applied pressure. Due to their simplicity of fabrication and device structure, low energy consumption in operation, and broad range of pressure detection, piezoresistive sensors have been intensively investigated. However, the sensing performance of most piezoresistive sensors suffers from poor sensitivity and cannot detect in low-pressure regimes. Capacitive sensors utilize the capacitance change due to contact from an external object. Though they have met with great commercial success, capacitive sensors applied on unstructured elastomeric dielectrics with small moduli have low compressibility and high viscoelasticity, leading to low sensitivity and slow response and relaxation time, respectively. Furthermore, to respond to variations in piezoelectric potential, capacitance, or resistance, most of these physical sensors are constructed from conductive polymers,^[22,24] metal nanowires,^[5–7] graphene,^[18,21,23,25] and carbon nanomaterials^[9,20] and possess complex micro- and nanostructures, such as pyramids,^[10,23] semispheres,^[22,24] and cylinders.^[6,7,26] However, the fabrication of these sensing elements is complicated, expensive, and time-consuming, requiring multiple steps and large-area integration of nanomaterial assemblies, which hinders industrial mass production. In addition, a majority of the above physical sensors are not fit for high energy consumption usage, and few designs involve the durability under washing that e-skins require. All these existing factors severely restrict the scope and depth for applications of functional e-skins.

As a new energy-harvesting and self-powered sensing technology, the developed triboelectric nanogenerator (TENG) can convert ubiquitous mechanical energy into electricity based on a coupled effect of contact-electrification and electrostatic induction,^[27–30] the output of which can be not only power source but also signals for self-powered sensor. Due to its high efficiency, light weight, low cost, environmental friendliness, and universal availability, it has promising applications in low-frequency mechanical energy harvesting and especially in multifunctional self-powered signal sensing.^[31–37] The integration of versatile TENG technology into functional e-skins brings new vitality and more possibilities for next-generation wearable electronics, personal healthcare, and human–machine interfaces.

Herein, we present a simple and low-cost method for fabrication of a stretchable and conformable skin-inspired TENG (SI-TENG) as a multifunctional e-skin, which is capable of simultaneously harvesting biomechanical energy and sensing mechanical stimuli. A continuous, planar, and “chain-link” fence-shaped interlaced conductive network constructed from zigzag distributed three-ply-twisted silver-plated nylon yarn is embedded into the silicone rubber elastomer, endowing the SI-TENG with adequate transparency, good stretchability, high pressure sensitivity, and excellent mechanical stability. The energy-harvesting SI-TENG with a dimension of $80 \times 40 \text{ mm}^2$ can generate an open-circuit voltage of 160 V and an instantaneous average power density of 230 mW m^{-2} , which is capable

of lighting up more than 170 light-emitting diodes (LEDs), charging commercial capacitors, and powering a digital watch. Due to its high pressure sensitivity and fast response time, the SI-TENG can monitor human physiological signals in real time, such as arterial pulse and voice vibrations. Furthermore, an intelligent prosthetic hand for finger tactile identification, a real-time pedometer and speedometer, and a self-powered soft digital keyboard are successively demonstrated in this paper to confirm its multifunctional applications. Furthermore, we demonstrate a stretchable tactile sensing array with a spatial resolution of 8×8 pixels that can detect and simultaneously map pressure distribution induced by normal mechanical stress. The developed yarn-embedded SI-TENG as a multifunctional e-skin has versatile applications in wearable electronics, humanoid robotics, wellness monitoring, and human–machine interfaces.

As triboelectric-based e-skin, appropriate material selection not only affects the fabrication process, but is also directly related to the final device performance. As we know, the triboelectric effect is a contact-induced electrification in which a material becomes electrically charged after it contacts a different material, and the sign of the charges carried by a material depends on its relative polarity in comparison to its counterpart.^[27–30] Therefore, one of the most effective strategies for enhancing TENG output performance is to select the appropriate paired tribomaterials with opposite triboelectric polarities from the triboelectric series. Compared with conducting nanomaterials and polymers, conductive fibers are an attractive platform for flexible and stretchable physical sensors because fibers are inexpensive, inherently flexible, shape-adaptive, and can be mass produced. In this article, a silver-coated nylon yarn with three-ply-twisted configuration is selected as the electrode due to its excellent electrical conductivity, mechanical robustness, and easy accessibility. Its surface morphology observed by scanning electron microscopy (SEM) is shown in **Figure 1a**. Elastomers with stretchable, transparent, and mechanical stable features are one of the desired packaging materials for e-skins.^[38–40] Herein, supersonic yet tough silicone rubber is chosen as the elastomeric dielectric, owing to its inherent biocompatibility, superior mechanical properties, excellent flexibility/stretchability, and strong tendency to gain electrons. As illustrated in **Figure 1a**, a continuous and interlaced conductive network with a “chain-link” fence configuration is constructed from a zigzag arranged conductive nylon yarn, which can provide a planar reticular sensing path for the SI-TENG. The conductive yarn network is uniformly distributed in the silicone rubber elastomer, endowing the SI-TENG with good transparency (lower right of **Figure 1a**). A basic cyclic unit with a rhombic structure is extracted from the conductive yarn network (top left in **Figure 1a**). The photographs of an actual SI-TENG and its partially enlarged view are displayed in **Figure 1b,c**, respectively. As shown in **Figure 1d**, the fabricated SI-TENG can conform to cover any complex curved surface, such as a human forearm, demonstrating its potential application for body-adaptive wearable electronics. Due to the inherent soft texture and flexible network structure of the SI-TENG, it can be stretched in any in-plane direction and can withstand arbitrary complex deformations, such as rolling up (**Figure 1e**). The excellent stretchability of the SI-TENG is attributed to the

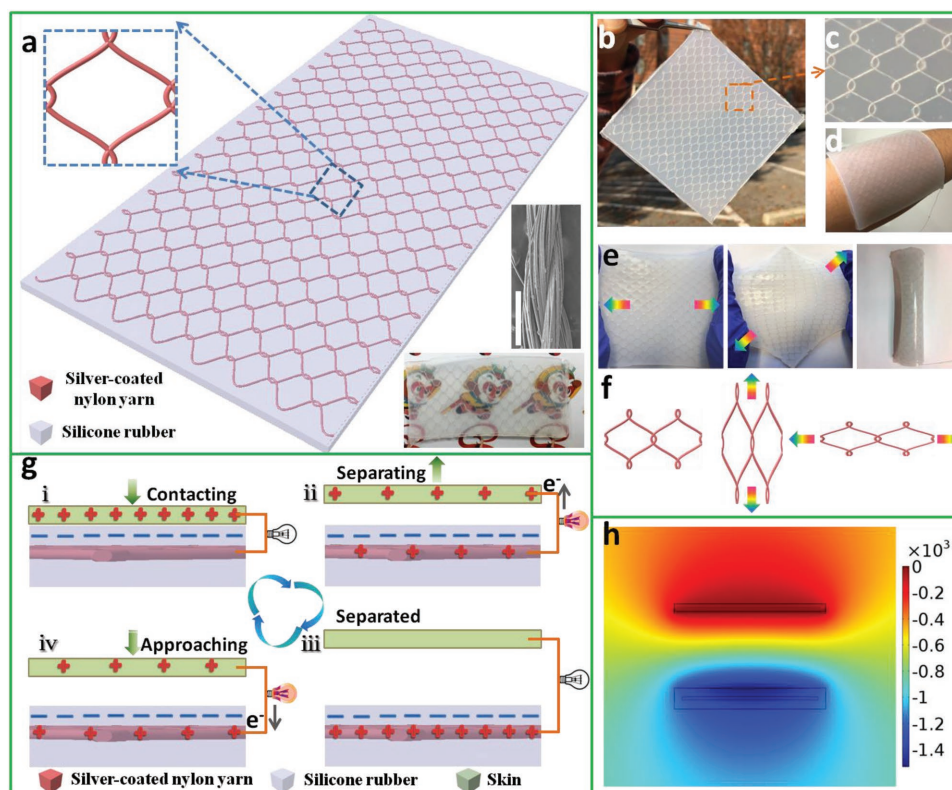


Figure 1. Structural design and working mechanism of the SI-TENG. a) Schematic illustration of the SI-TENG with “chain-link” fence-shaped structure and rhombic unit design. A basic repeated rhombic unit of the yarn conductive network is enlarged in its top left. An SEM image of the surface morphology of the three-ply-twisted silver-coated nylon yarn is presented on the right (Scale bar: 400 μm). The transparency of the SI-TENG is shown on the lower right. b) Photograph image of an actual SI-TENG and c) its partially enlarged view. d) Photograph showing that the SI-TENG can conformably attach to an individual’s forearm. e) Photograph showing that the SI-TENG can be stretched in any in-plane direction and even be rolled up. f) Schematic demonstrating the in-plane tensile behaviors of the repeated rhombic unit in the SI-TENG system. g) Schematic of the operation mechanism of the SI-TENG in single-electrode mode. h) Numerical calculation of the potential distribution of the SI-TENG at the maximally separated state by using COMSOL software.

zigzag yarn arrangement and rhombus interlaced network. As illustrated in Figure 1f, when the SI-TENG is subjected to external tensile loading, the zigzag arranged yarn gradually straightens and the rhombic region gradually extends along the tensile direction to adapt to external loading. The stretchability of the SI-TENG mainly depends on the basic structure parameters (the height h and the length l , Figure S1, Supporting Information) of the conductive yarn network and the thickness (d) of silicone rubber. When the h and l are equal to 1.24 mm and d is 2.8 mm, the stretchability of SI-TENG can reach 30%. It must be noted that the human arm skin can endure a maximum strain of $\approx 27\%$.^[41] Therefore, the present SI-TENG system is capable of performing desirably under common physical conditions of the epidermis. Moreover, the transparency of the SI-TENG can be improved through decreasing the values of h , l , and d (Figure S2, Supporting Information). The detailed fabrication methods of the SI-TENG are further introduced in Figure S3 (Supporting Information) and in the “Experimental Section.”

The working principle of the SI-TENG is illustrated in Figure 1g, which is based on a coupled effect of contact electrification and electrostatic induction. Note that the human body, which is a good conductor, serves as the ground for all

wearable TENGs. In our SI-TENG system, if the embedded yarn electrode is connected to human skin (i.e., the ground) through the external load, the SI-TENG will work in a single-electrode mode and human skin can be regarded as another triboelectric electrode.^[42] The relative motion of one cycle can be simplified as a contact-separation process that occurs between the SI-TENG and human skin. Once the skin contacts with silicone rubber, electrification occurs at the interface and generates the same amount of charges with opposite polarities at the surface of the skin and silicone rubber, respectively (Figure 1g-i). The silicone rubber is proven to be negatively charged because of its ability to attract more electrons than human skin and the silver. Because the two opposite charges coincide at almost the same plane, there is practically no electrical potential difference between the two surfaces. When the two surfaces are separating and gradually moving away, positive charges will be transferred from human skin to the inner yarn electrode due to the electrostatic induction effect. The accumulated electrical potential difference between human skin and inner yarn electrode prompts electrons to flow, generating an instantaneous electrical current (Figure 1g-ii). When the two triboelectric layers are separate from each other, the negative triboelectric charges on the silicone rubber are fully equilibrated by the induced

charges in the yarn electrode. Under complete separation, electrical signal is absent at the triboelectric layers' surfaces, reflecting the neutralization of both the positive and negative charges in this period (Figure 1g, iii). It should be noted that the accumulated charges will not be entirely annihilated. Instead, they will be maintained for a sufficiently long time because of the innate features of insulator. In the reverse case, if the skin is approaching back to the SI-TENG, the accumulated positive charges in the yarn electrode flow back to the human skin side through the external load to compensate for electrical potential differences (Figure 1g, iv). After the whole system returns to the contact state (Figure 1g, i), the negative charges of the silicone rubber are fully offset by the positive charges on human skin again. As a result, a contact-separation process between human skin and the SI-TENG will generate an instantaneous alternating potential and current through the external load. To obtain a more quantitative understanding of the electricity generating process, we established a theoretical model of the SI-TENG to observe the electric potential distribution of every component under the fully separated state by a simple finite element simulation using COMSOL Multiphysics (Figure 1h).

The electrical output performance of the SI-TENG, including open-circuit (OC) voltage (V_{OC}), short-circuit (SC) current (I_{SC}), and short-circuit (SC) charge transfer (Q_{SC}), is quantitatively measured by a mechanical linear motor. Before fabricating the final device, the electrode materials and structural parameters of the SI-TENG are discussed in advance. In this paper, other kinds of frequently used electrodes for SI-TENGs, including silver-coated conductive nylon fabric, Ag nanowires (AgNWs), carbon nanofibers (CNFs), copper mesh, thick (0.1 mm) and thin (0.01 mm) copper foil, are also embedded in the silicone rubber (Figure S4, Supporting Information). Furthermore, four types of yarn-embedded SI-TENGs are tested to investigate the effect of h and l on the electrical output performance of SI-TENG. For simplifying structure as well as facilitating analysis, the h is assumed to be equal to the l , which is varied at 2.24, 3.24, 5.24, and 10.24 mm, respectively. The thickness and dimensions of these devices are well controlled to make them as consistent as possible, which are 2.8 mm and $80 \times 40 \text{ mm}^2$, respectively. According to their electrical outputs in Figure 2a–c, the yarn embedded SI-TENG with the h and l of 3.24 mm shows the best electrical output performance when compared with others. The excellent output performance of the single-electrode mode SI-TENG can be attributed to two main reasons, which are relating to the special yarn network structure. On one hand, for a fixed size of TENG, when its electrode area (S) is sufficiently small, Q_{SC} has been proven to be proportional to S . However, when S is large enough, the Q_{SC} shifts downward dramatically, which shows that the charge transfer efficiency decreases significantly when S is large.^[30,42] Therefore, there is a suitable electrode area for TENG to reach the optimal electrical output performance, which is the SI-TENG with the h and l of 3.24 mm in this work. On the other hand, the yarn arranged back and forth constitutes numerous parallel-connected conductive paths in the SI-TENG. As we know, for single-electrode mode TENG, parallel connection is another effective way to scale up the output.^[42] However, the enhanced effect is related to the unit space. When the spacing is small, the electric field from each unit will be interfered, resulting in a decrease of

output. Only when their spacing is large enough, the mutual influence will be minimized. Therefore, a large enough spacing is critical for the scale-up of the output for parallel connection. This may explain why the SI-TENG with h and l of 3.24 mm possesses the highest output among the four types. The more detailed analyses about the two reasons are presented in Note S1 (Supporting Information). As the thickness of the silicone rubber increases, the electrical outputs of the SI-TENG initially rapidly increase, then decrease, and finally stabilize (Figure S5, Supporting Information). If the coverage of silicone rubber is not enough for the entire yarn electrode, the electrical output capability of the SI-TENG is weakened due to charge leakage. After the coverage of silicone rubber exceeds a certain amount, the electrical output performance of the SI-TENG can be greatly enhanced. However, with continued increase in silicone rubber thickness, the capacitance between the skin surface and yarn electrode decreases, resulting in a lower electrical output. The stress-strain curves of the SI-TENG with h and l of 3.24 mm further verify its excellent tensile capability (Figure S6, Supporting Information). After the tensile strain of the SI-TENG reaches $\approx 160\%$, yarn slippage occurs, resulting in its failure. The electrical outputs of the SI-TENG under several tensile strains (i.e., 5, 10, 15, and 20%) are also measured at a fixed striking force of 20 N (Figure S7, Supporting Information). Although the electrical outputs of the stretched SI-TENG decrease compared with the values of the original state, they almost stabilize without further reduction at higher tensile strains.

The frequency response of the SI-TENG with optimal structural parameters (i.e., h and l are 3.24 mm, and d is 2.8 mm) is further discussed (Figure 2d–f). When the striking frequencies increase from 1 to 5 Hz, the peak V_{OC} and Q_{SC} are nearly stable ($\approx 160 \text{ V}$ and $\approx 60 \text{ nC}$, respectively). On the other hand, the I_{SC} increases from 0.55 to 2 μA , revealing a clearly enhanced trend with the increase of contact frequency. In other words, the increase of frequency is favorable for the magnitude of I_{SC} . The average current densities I of the yarn-embedded SI-TENGs are also measured by connecting them with variable resistors R in series. And thus, their average power density P can be obtained as $P = I^2 R/A$, where A is the effective contact area. Due to Ohm's law, with the exponential increase of R , all the I represent a trend of initial stability and then a rapid decrease (Figure 2g). All the P of the yarn-based SI-TENGs reach their peak values at a resistance of about 1 $\text{G}\Omega$ (Figure 2h). Similar to the results in Figure 2a–c, the yarn-based SI-TENGs with h and l of 3.24 mm, whose peak power density is 240 mW mm^{-2} , have the highest power outputs. The long-term stability and durability of the SI-TENG have been demonstrated. As shown in Figure 2i and Figure S8 (Supporting Information), almost no significant decreases of the V_{OC} and I_{SC} are found even after 50 thousand continuous loading cycles, clearly demonstrating its significant robustness and practical value. For wearable e-skins, washing durability is an essential requirement for their long-term usage. In our SI-TENG system, both the conductive yarn and silicone rubber are washable and mechanically robust. Therefore, the whole system is washable and can withstand complex mechanical agitation. In this work, the washability of the SI-TENG is tested under a simulated domestic laundering environment with household detergent and a magnetic stir bar added (Figure S9a, Supporting Information). Each laundering cycle

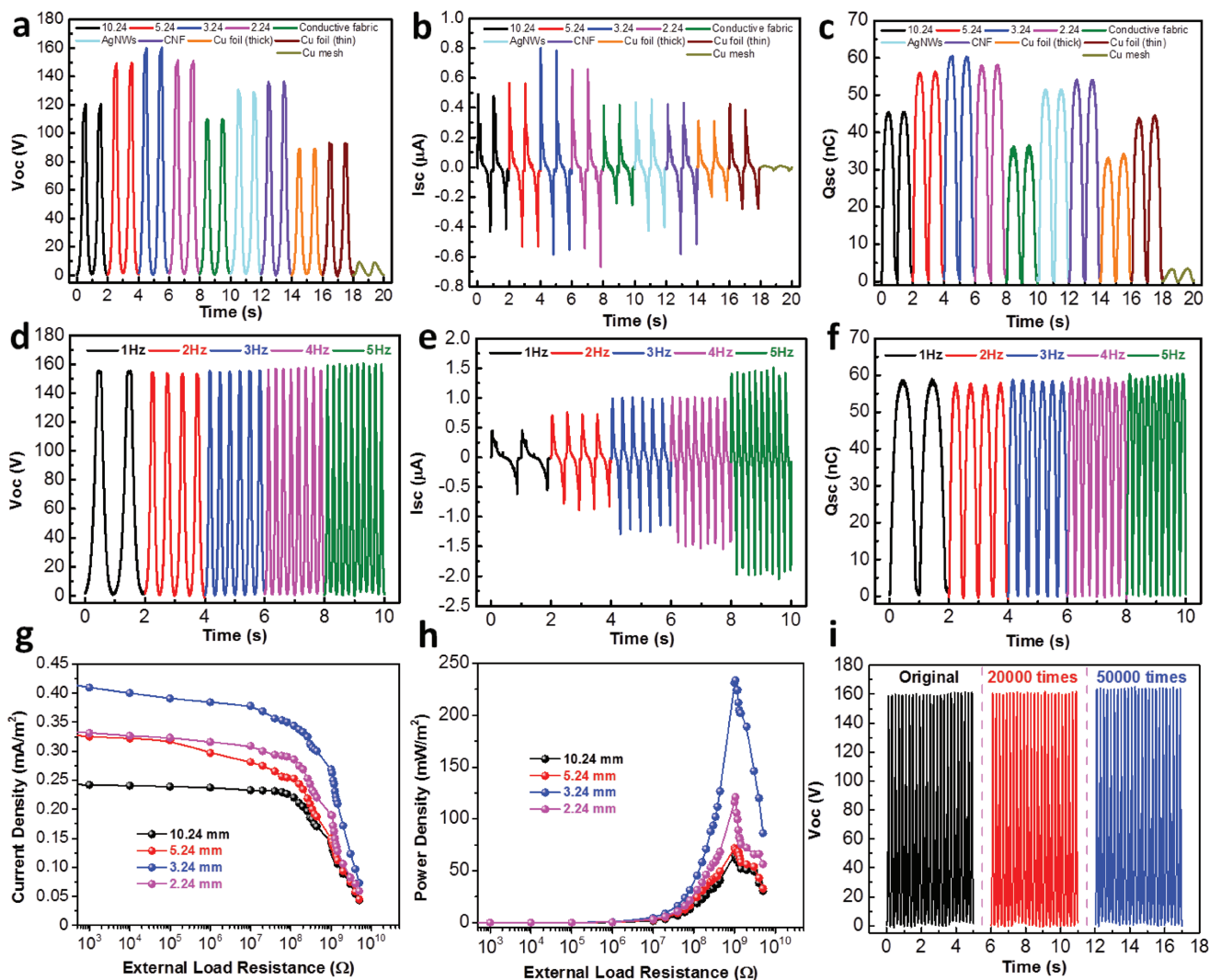


Figure 2. Electrical output performance of the SI-TENG. a–c) Effect of embedded electrodes on the electrical output performance including: a) V_{OC} , b) I_{SC} , and c) Q_{SC} of the SI-TENGs. In addition, according to the height h and length l of the zigzag arranged conductive yarn, four types of yarn-based SI-TENGs with the h and l of 2.24, 3.24, 5.24, and 10.24 mm are designed. d) V_{OC} , e) I_{SC} , and f) Q_{SC} of the SI-TENG under different loading frequencies (1–5 Hz). g) Variation of the instantaneous output current density and h) power density with external resistances. i) Long-term stability and durability test of the SI-TENG.

lasts 20 min, and the spinning velocity of the magnetic stirrer is controlled at 600 rpm. After running each cycle and drying naturally, the V_{OC} and I_{SC} under different washing times are measured, as shown in Figure S9b,c (Supporting Information), respectively. The capability to harvest mechanical energy is well maintained without significant decline, clearly indicating the good washing durability of the SI-TENG. All these excellent properties of our SI-TENG make it a good candidate for biomechanical energy harvesters and versatile self-powered sensors.

Due to the excellent electrical output performance of the SI-TENG, it can first be used as a wearable power source for biomechanical energy harvesting. The embedded yarn electrode endows our SI-TENG with diversified pattern designs, such as alphabets, numbers, or flowers (Figure S10, Supporting Information). Different yarn patterns will not affect the electrical output performance of the SI-TENG, as proved in Figure S10d–f (Supporting Information). A letter-shaped

SI-TENG with a marked pattern spelling “TENG” can be fabricated by yarns with different colors (Figure 3a). If the letter-shaped SI-TENG is further cut into four independent letter buttons, each of these buttons can individually light up a corresponding LED array (Figure 3b and Movie S1, Supporting Information). This feature inspires us to design it as a flexible smart keyboard, which will be introduced below. Under normal hand patting, an SI-TENG with a dimension of $80 \times 40 \text{ mm}^2$ can instantaneously light up more than 170 LEDs, and even when it is stretched (Figure 3c,d, Movie S2, Supporting Information). The electricity harvested from the SI-TENG can be further stored in energy storage devices (e.g., capacitor and battery) for later usage. The effects of striking frequency (1–5 Hz) and capacitance capacity (1–22 μF) on the charging ability of SI-TENG are also investigated. The charging velocity of the SI-TENG increases with the increase of striking frequency (Figure 3e). However, with an increase in capacitance,

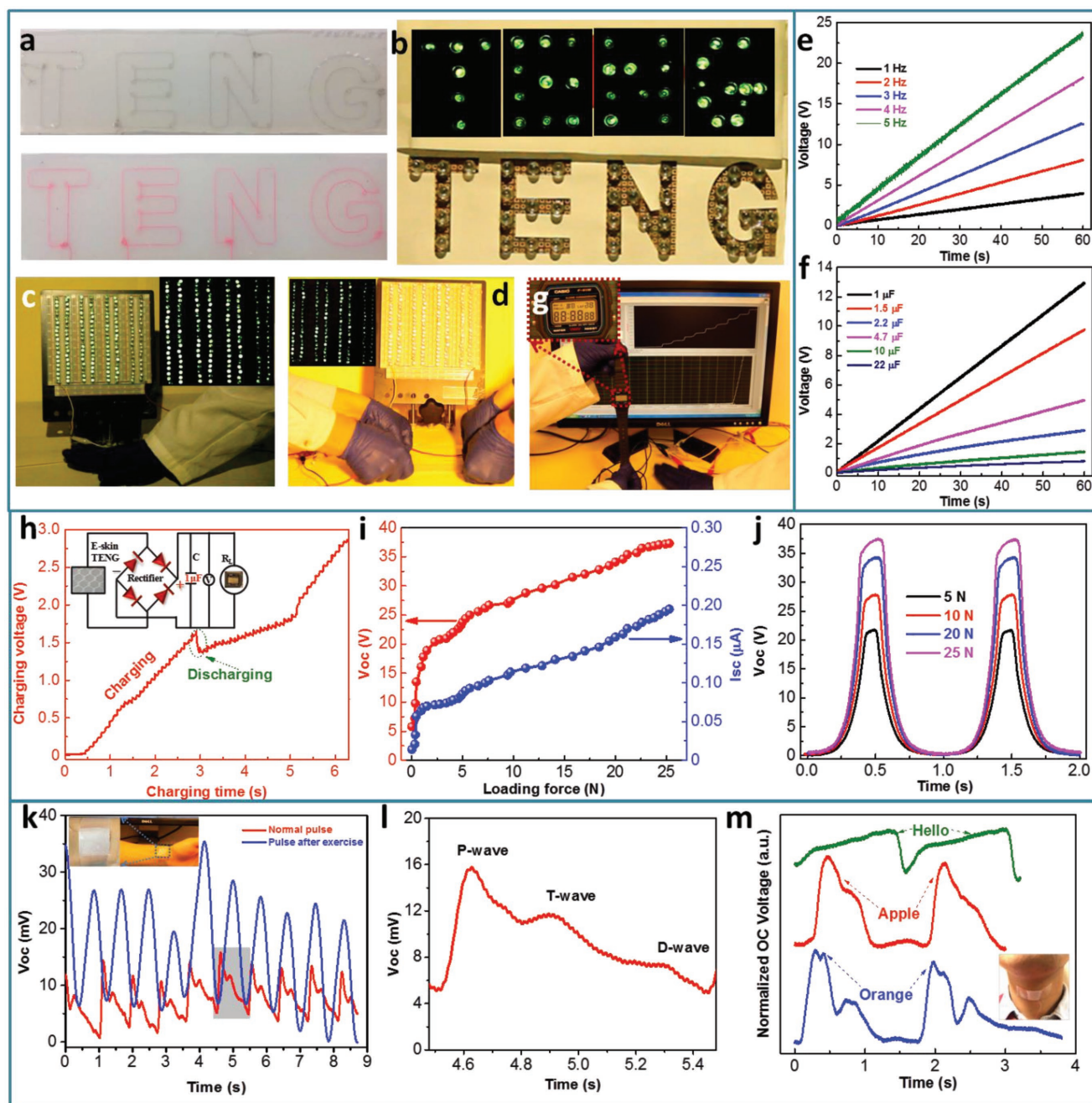


Figure 3. Energy-harvesting capability, pressure sensitivity, and physiological monitoring application of the SI-TENG. a) Photograph of the SI-TENG marked as alphabets with grey or red conductive yarns. b) Demonstration of lighting up different LED units by tapping the SI-TENGs with corresponding letters (each size: $30 \times 30 \text{ mm}^2$). c,d) Demonstrations of lighting up 170 LEDs by tapping the SI-TENG at normal (c) and stretching (d) states (size: $80 \times 40 \text{ mm}^2$). e,f) Charging capability of the SI-TENG under different striking frequencies (1–5 Hz) (e) and under different capacitance capacities (1–22 μF) (f). g) Demonstration of powering a commercial watch by hand tapping the SI-TENG. Inset is the enlarged view of the working watch screen. h) Charging voltage of the SI-TENG as a function of charging time. Inset is the circuit diagram of the charging system. i) Variations of OC voltage and SC current of the SI-TENG as a function of loading force. j) Response of the SI-TENG-based pressure sensor with various applied loadings (5, 10, 20, and 25 N). k) Real-time arterial pulse waves under normal and exercise conditions. Inset is the photograph of a pressure sensor attached on a wrist. l) Single signal waveform extracted from the marked region in (k). m) Recognition of sound signals when the wearer spoke “Hello,” “Apple,” and “Orange.” Each word was spoken twice. Inset is the photograph of a sensing unit firmly mounted on a volunteer’s throat for monitoring his muscle movement during speech.

a slower charging velocity will be found (Figure 3f). The stored electricity in a capacitor can sustainably power various miniaturized wearable electronics, such as an electronic watch

(Figure 3g and Movie S3, Supporting Information). Figure 3h presents the recorded voltage versus time curve during this charging process. The watch starts to work after the charging

voltage reaches its threshold value, which needs about 2.5 s. Although the voltage undergoes a rapid discharging process, it can be charged up again if the device is flapped continually. From these analyses, it is found that the SI-TENG can provide enough power for most wearable electronics, which makes it an excellent choice as a potential power source.

To study the pressure sensitivity of the SI-TENG, its electrical outputs as a function of loading forces are investigated. As shown in Figure 3i, V_{OC} and I_{SC} increase with the increase of applied loadings. Also, both of them present an approximate linearly increasing trend after the force exceeds about 2 N. As shown in Figure 3j, the V_{OC} signal profiles are regular and replicable even when the loading force increases to 25 N. Due to the high pressure sensitivity, the SI-TENG is able to detect subtle physiological signals, such as arterial pulse wave and voice vibrations. By sticking an SI-TENG ($20 \times 20 \text{ mm}^2$) on a volunteer's wrist (inset in Figure 3k), real-time arterial pulse voltage signals with regular and repeatable pulse shapes are monitored under different body conditions (e.g., normal and exercise in Figure 3k). It can be found that the pulse frequencies under normal and exercise states are 67 and 88 beats per minute, respectively. A typical arterial pulse signal extracted from Figure 3k contains three distinct waves, i.e., percussion wave (P-wave), tidal wave (T-wave), and diastolic wave (D-wave), which are related to the systolic and diastolic blood pressure, the ventricular pressure, and the heart rate, respectively (Figure 3l).^[43,44] The arterial pulse waves can also be represented as real-time short-circuit current signals, as demonstrated in Figure S11 and Movie S4 (Supporting Information). Voice recognition is also investigated by attaching an SI-TENG ($20 \times 20 \text{ mm}^2$) on an individual's throat (inset in Figure 3m). According to the voltage signals generated from sound vibration, the SI-TENG can distinguish differences between the spoken words such as "Hello," "Apple," and "Orange" quickly and accurately (Figure 3m). Note that each word is spoken at least twice for repeatability test. Therefore, it might be useful for people with damaged vocal cords to rehabilitate their speech ability by training to control their throat muscle movement. Our SI-TENG-based sensor relying on the deformation of epidermis and muscles provides an interesting and effective method for physiological monitoring, which can be used for noninvasive disease diagnosis and personal healthcare.

Based on the high pressure sensitivity of the SI-TENG-based sensor, an intelligent prosthetic hand for finger tactile identification is demonstrated. Five independent SI-TENG-based pressure sensors with the same dimensions of $10 \times 8 \text{ mm}^2$ are sewn on the five fingertips of a glove, respectively. As shown in the top of Figure 4a, a hand wearing this glove touches different objects with different fingertip configurations, such as keeping all fingers straight, holding a pen with the first two fingers, clicking a mouse with the first three fingers, grasping a beaker with the last three fingers, and holding a beaker with all fingers. According to the number of contacted fingers, the corresponding hand gestures (bottom in Figure 4a) will be transformed and identified in the self-developed output interface. When a finger touches external object, a real-time voltage signal will be generated. In other words, through the SI-TENG-based sensor, instantaneous finger tactile actions are converted into readable, quantized, and real-time electrical signals. When

a tester wearing the glove-shaped sensors successively conducts the five actions (Figure 4a), the corresponding real-time voltage signals of the five fingers are recorded in Figure 4b. This process is further demonstrated in Movie S5 (Supporting Information). It is found that a reverse voltage peak occurs if a finger contacts an object. However, no or a small forward voltage peak is found when the finger is not in contact with an object. The small positive voltage peaks of the noncontacting fingers are attributed to the co-movement influence of the contact fingers. In addition, the hand gestures are consistent with and specific to the generated voltage signals. For example, when the hand holds a beaker with all the five fingers, five real-time reverse voltage signals appear and the corresponding hand gesture of making a fist presents in the self-developed software output interface (Figure 4c). The self-developed software output interface of the intelligent prosthetic system includes a real-time voltage output window and hand gestures transformed images. In summary, the developed intelligent prosthetic hand could allow amputees or individuals with nerve damage to gain artificial sensing in order to improve rehabilitation and transform the lives and abilities of the disabled patients.

A pedometer/speedometer records step number, motion speed, travelled distance, and even consumed calories, which make it very popular among athletes and running enthusiasts. Based on the energy harvesting and high sensing features of the SI-TENG, a self-powered and real-time pedometer/speedometer is developed in this paper. As we know, in the course of human walking, the maximally contacted area with the ground is the heel. Therefore, to enhance the final electrical signal outputs as well as make the signal characteristic more obvious, the SI-TENG is sewn on the heel of a sock (Figure 4d). In addition, in order to compare the electrical signal differences between left and right feet, two SI-TENGs with the same dimension of $20 \times 20 \text{ mm}^2$ are placed on the left and right feet, respectively. While switching between the three main states (i.e., standing, walking, and running, Figure 4e) of human activity, the real-time voltage signals of the left and right feet are recorded in Figure 4f. All the curves present sinusoidal alternating electrical signals, which is due to the periodic contact separation movements between human feet and the ground. In the course of running, the SI-TENG on the heel contacts more fully with the ground than that during walking, resulting in a higher voltage output of running. Furthermore, the motion frequency of running is faster than that of walking. Due to the opposite movement states of left and right feet, their voltage signals also exhibit a reversely varying trend. When a foot is flat on the ground, the SI-TENG contacts the ground and generates an inverse voltage signal (trough). On the contrary, if the foot is raised, the SI-TENG separates from the ground resulting in a forward voltage signal (peak). The step number and motion speed can be obtained, according to the collected voltage signals of the two SI-TENGs. The step number (n) is easily calculated based on the number of voltage peaks or troughs. Here, it is assumed that the step lengths (L) of an adult male in the walking and running states are 0.7 and 1 m, respectively. Therefore, the travelled distance (s) of human motion can be obtained as $s = n \times L$. The step frequency per hour (f) can be expressed as $f = 3600/t$, where t is the time consumed by each step. Therefore, the average motion speed per hour (v) can be

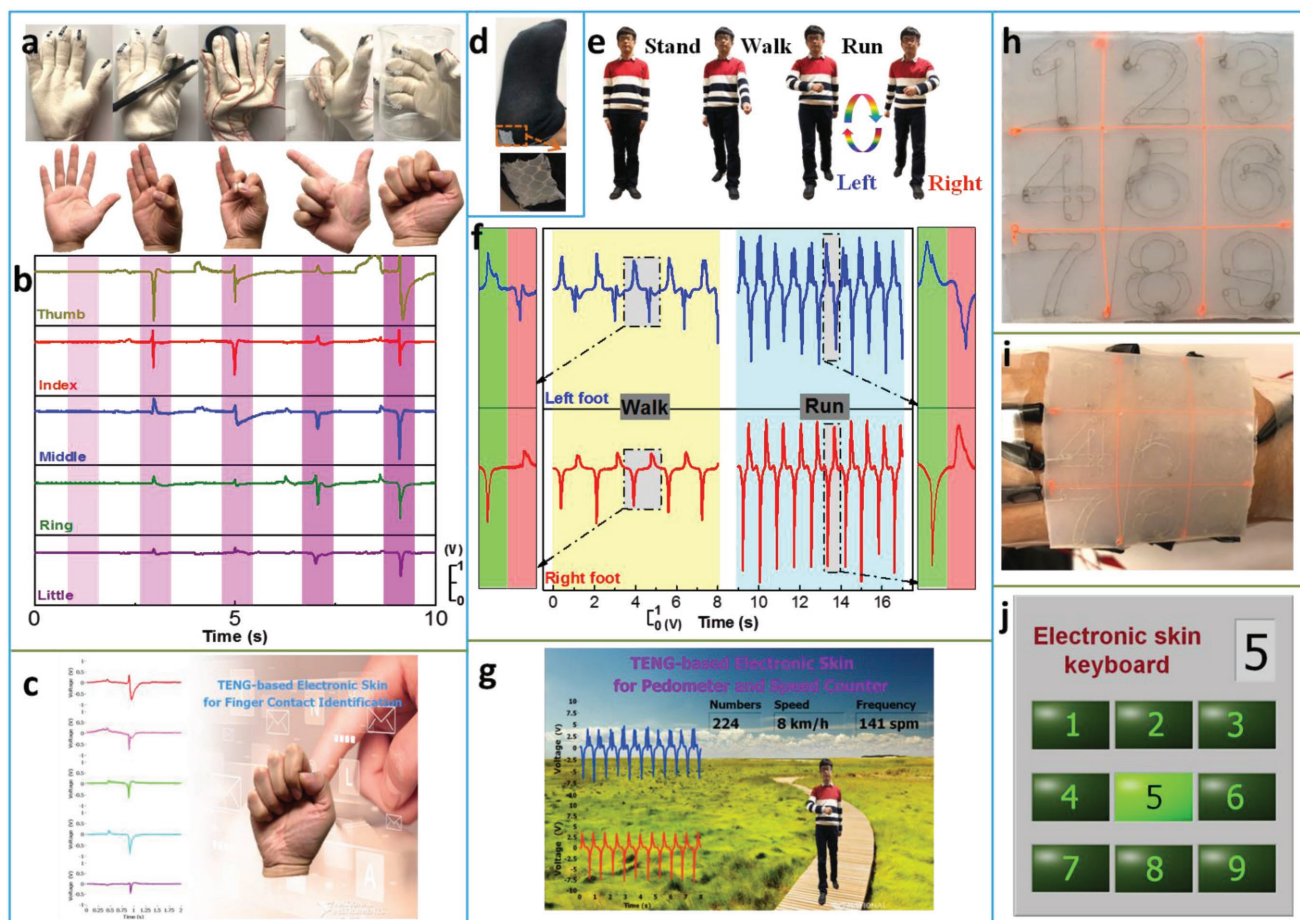


Figure 4. Applications of the SI-TENG-based pressure sensor as an intelligent prosthetic hand, a self-powered pedometer/speedometer, and a flexible digital keyboard. a) Photograph of a glove with five pressure sensors implanted on its fingertips. The top is the glove holding different objects, and the bottom is the corresponding hand gestures. b) Real-time voltage signals of the five independent pressure sensors in response to five different hand motions. c) The developed output interface for the personalized intelligent prosthesis. d) Photograph showing an SI-TENG sewn on the heel of a sock. e) Photographs demonstrating the different motion states of an individual, including standing, walking, and running. f) Real-time voltage signals of the two SI-TENGs (attached on left foot and right foot, respectively) during the process of walking and running. g) Software output interface of the self-powered pedometer and speedometer. h) Photograph of a flexible digital keyboard with nine key buttons. i) Photograph demonstrating that the flexible digital keyboard is conformably attached on a personal forearm. j) Digital display interface for the self-powered digital keyboard.

further calculated as $v = L \times f$. The software output interface of the self-powered pedometer/speedometer is presented in Figure 4g, which includes two real-time voltage signals from the left and right foot, the windows for the step number, the motion speed, the step frequency, and the image of athlete. The demonstration of the self-powered pedometer and speedometer is presented in Movie S6 (Supporting Information).

With the rapid development of wireless communication and wearable electronics, human-machine interfacing devices must be portable, compatible with wearable systems, and robustly sealed against contaminants. To meet these requirements, a soft, planar, and yarn-based digital keyboard with flexible, stretchable, conformable, and self-powered features is designed for wearable user input interfaces. As shown in Figure 4h, conductive yarn keys in the form of numbers (1–9) are embedded inside silicone rubber and adjacent number keys are further separated by nonconductive yarn to minimize their mutual interference. Note that the typical human finger is ≈ 2 cm wide, necessitating keyboards with dimensions

within the order of tens of centimeters. Therefore, the dimension of each key in the portable alphanumeric keyboard is set as 20×20 mm². The developed keyboard is light-weight, highly flexible, stretchable, and can conformably cover complex curved faces, such as the human forearm (Figure 4i). When a key is pressed, an instantaneous electrical signal is produced. The interference electrical signals from other non-contact keys can be effectively excluded by setting a certain threshold. If the electrical signal of the pressed key exceeds the threshold, the corresponding digital indicator in the user interface will be lit up, as demonstrated in Figure 4j and Movie S7 (Supporting Information). The flexible digital keyboard can still work even when it is adhered on a human forearm (Movie S8, Supporting Information). These demonstrations confirm that our SI-TENG-based keyboard made from conductive yarn electrodes embedded in flexible elastomer introduces a simple, low-cost and efficient method to design flexible and stretchable keyboards. Moreover, this work contributes to the field of stretchable electronics by paving the way for the facile

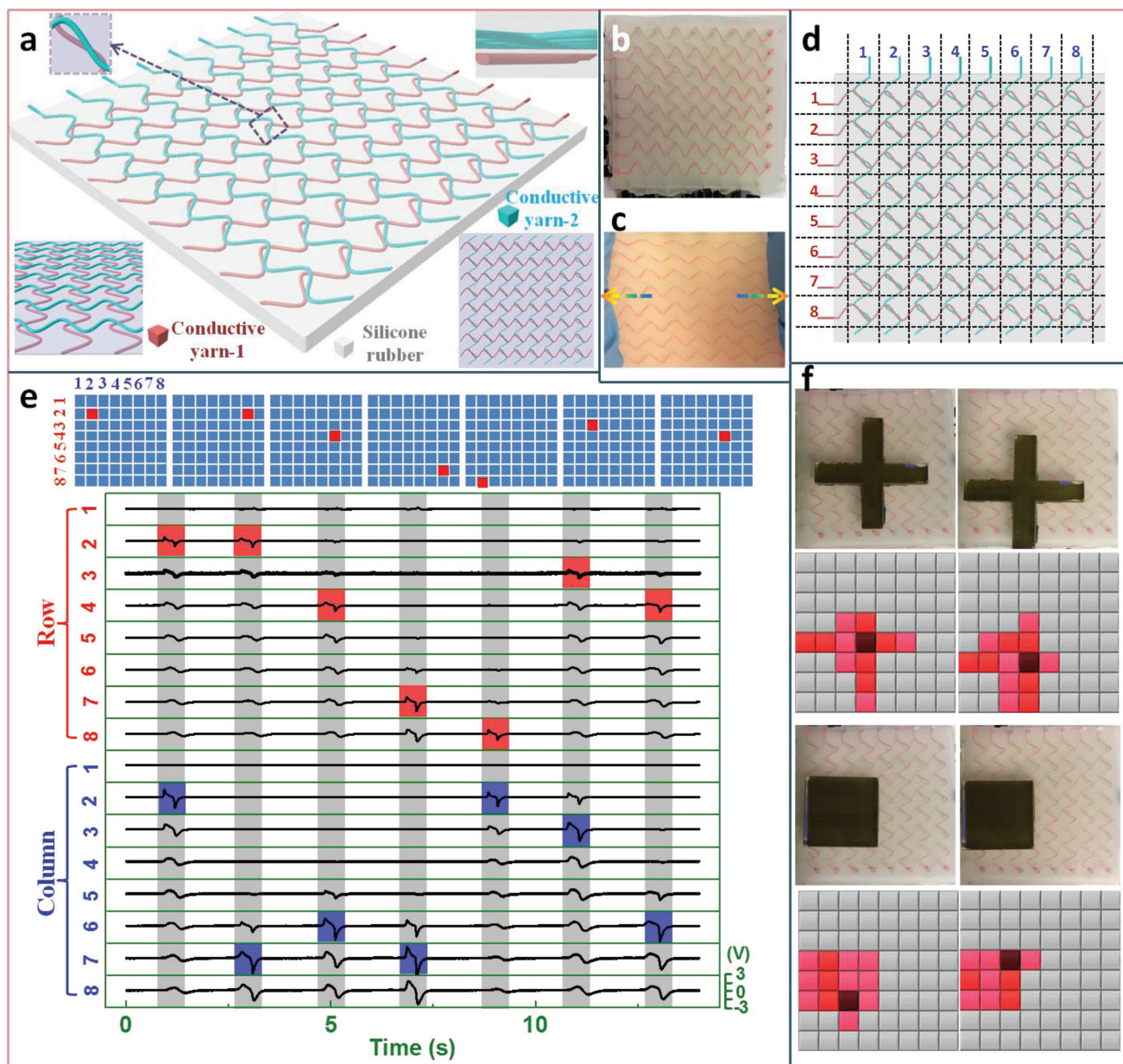


Figure 5. Application of the SI-TENG-based pressure sensor as a stretchable tactile sensing array. a) Schematic illustration of the SI-TENG-based tactile sensing array. A basic sensing pixel, a cross-section view, a partially enlarged oblique view, and the front view of the tactile sensing array are distributed in its top left, top right, lower left, and lower right, respectively. b) Photograph of the fabricated SI-TENG-based tactile sensing array. c) Photograph demonstrating the tensile behavior of the SI-TENG-based tactile sensing array. d) Schematic demonstrating that the SI-TENG-based tactile array is divided into 8×8 sensing pixels. e) The real-time voltage signals of each pixel and the finger touching positions displayed in the output interface. f) Photographs of the SI-TENG-based tactile sensing array with rectangular and cross-shaped blocks placed on top and their corresponding planar pressure intensity profiles in the sensing array.

and larger-area fabrication of wearable human–machine interfacing devices.

As for electronic skins, the capability of integrating multiple sensors to form a large-area and low-cost flexible sensor array with excellent performance is desired for detection of spatially resolved pressure. To this end, a proof-of-concept SI-TENG-based pressure sensing array with 8×8 spatial pixel resolution is also fabricated. The detailed fabrication processes of the SI-TENG-based pressure sensing array are introduced in

Figure S12 (Supporting Information) and in the “Experimental Section.” As illustrated in Figure 5a, eight serpentine conductive yarns are arranged in the top (column, marked as x) and bottom (row, marked as y) layers of the sensing array, respectively. Each yarn is vertically intersected with all the yarns of the other electrode layer, constituting a cross network structure. All sixteen conductive yarns are further embedded in the silicone rubber, endowing the device with integrity and washability. An overlapping region between the row and column

yarns constitutes a basic sensing unit of the tactile sensing array (top left in Figure 5a). A middle dielectric layer separates the top and bottom electrode layers in order to prevent electrical signal interference between them (top right in Figure 5a). Therefore, the output signals from the top and bottom layers are independent, meaning that each sensing unit is connected to two independent channels. In addition, to reduce the cross talk between adjacent pixels, adjacent yarns of the same electrode layer are also separated by silicone rubber. As shown in Figure 5b, an SI-TENG-based tactile sensing array with dimensions of $60 \times 60 \text{ mm}^2$ is fabricated, which is stretchable, bendable, twistable, and can be conformably attached to a human wrist (Figure S12, Supporting Information). Upon stretching, the serpentine yarns gradually straighten for adapting to the deformation of the elastomer (Figure 5c). If the external tensile force is released, the tactile sensing array can easily and quickly return to its initial position without residual deformation. According to the overlapping positions of the top and bottom yarn electrodes, the 8×8 sensing array can be divided into 64 units (Figure 5d). The symbol of the sensing units are marked as ij ($i, j = 1, 2, \dots, 8$), where i and j represent the serial number of top and bottom electrodes, respectively. The generated voltage signals of the top and bottom electrode layers are denoted as x_i and y_j ($y_j \leq x_i$), respectively. As discussed above, each sensing unit corresponds to two independent voltage signals, which are from the top and bottom electrode layers, respectively. Under normal circumstances, the maximum voltage signals should be from the load applied positions. For single-point contact, the contact point can be easily locked in the sensing array by finding the maximum voltage signals in the column (x_{\max}) and row (y_{\max}), respectively. For example, when a finger contacts the sensing units, the real-time voltage signals of the 16 channels are shown in Figure 5e, where the maximum voltage signals of the row and column are highlighted in red and blue, respectively. Therefore, the intersections of x_{\max} and y_{\max} can be regarded as the finger contact regions, such as 22, 72, 64, 77, 28, 33, and 64, which are marked in red in the top of Figure 5e (Movie S9, Supporting Information). The reliability and repeatability of the method are also investigated. As shown in Figure S14 (Supporting Information), when the key at the 88 position is pressed three consecutive times, the similar voltage output signals testify its good reliability and repeatability. For multipoint contacts or regional mapping, the distributed contours of the loading objects are determined based on the sum of voltage signals (n) from the column (i) and row (j) electrode layers, which can be represented as $n = x_i + y_j$. Due to the uneven surface of the loading objects and the inconsistent applied pressure to the device, the generated voltage signals of different sensing units are also different. Based on this finding, the loading intensity from external objects can also be observed in the tactile sensing array. The maximum n (i.e., m , $m = x_{\max} + y_{\max}$, $n \leq m$) in the contact region can be first obtained by picking out the x_{\max} and y_{\max} . For other contact units, the maximum voltage attenuation rule is used to determine whether a sensing unit has pressure applied or not and the pressed degree of the contact units. The attenuated voltages p are determined based on the equation as $p = [(n/m)q]$, where q refers to the magnification coefficient of voltage signals and the square bracket represents integer function. If the n of a sensing unit is lower than a set threshold, it

can be considered to be in noncontact with external objects. In our demonstration, six levels of color contrast are designed to display the pressed degree of the contact units, in which the deeper the color is, the greater the pressed degree will be. For example, when a square-shaped or cross-shaped acrylic plate is placed on the sensing array, the presented color contrast maps have a good consistency with the shape of the applied objects (Figure 5f, Movies S10 and S11, Supporting Information). It is also necessary to note that the resolution of the sensor arrays can be conveniently tuned by changing the number or the size of the sensing units. The SI-TENG-based tactile sensing array represents a facile, reliable and self-powered candidate for artificial e-skins, which holds promising applications in human-machine interfaces such as multitouch devices.

In summary, a stretchable and conformable SI-TENG as a multifunctional e-skin is developed through a simple, low-cost, and easily scalable approach. A planar yarn conductive network constructed from a zigzag arranged three-ply-twisted silver-coated nylon yarn is embedded in a silicone rubber elastomer. The special "chain-link" fence-shaped structure endows the SI-TENG with desired stretchability, good sensitivity, high detection resolution, and fast response time. The energy harvesting and multifunctional sensing properties are well combined in the SI-TENG to achieve a good complement of their respective advantages. As an energy harvester, the SI-TENG can generate an instantaneous average power density of 230 mW m^{-2} , and is capable of lighting up 170 LEDs, sustainably charging capacitors, and powering an electronic watch. As a self-powered sensor, the SI-TENG can monitor human physiological signals in real time, such as wrist pulse detection and voice recognition. Furthermore, a personalized intelligent prosthesis, a real-time pedometer/speedometer, and a self-powered flexible digital keyboard are also successively demonstrated to further confirm its excellent sensing performance. Finally, an SI-TENG-based pressure sensing array with 8×8 spatial pixel resolution that is able to simultaneously map and quantify mechanical stresses induced by pressure is also proposed and demonstrated. We envision that our self-sustainable SI-TENG with excellent biomechanical energy harvesting capability and versatile pressure sensing properties has potential applications in wearable artificial skin for wearable power sources, humanoid robotics, biomedical prostheses, physiological monitoring, self-powered motion sensing, and human-machine interfacing devices.

Experimental Section

Preparation of Serpentine Yarn Electrode: In this work, a three-ply-twisted silver-coated nylon yarn (nominal diameter: $180 \mu\text{m}$, resistance $<100 \Omega \text{ cm}^{-1}$, LessEMF.com) was selected as the electrode material; an acrylic plate was selected as the substrate material; and nails were used to fix the yarn's position. First, uniform and regular holes with the diameter of 1.24 mm were distributed in the acrylic plate by laser cutting. Then, nails were put into these preset holes. The nail heads on the acrylic plate were further fixed by transparent tape to prevent them from falling off. Afterward, the conductive yarn was twined around the nails to form a serpentine configuration. After winding back and forth, a planar and continue conductive network with a rhombus basic unit was finally obtained. It is also worth noting that the arranged density of the conductive network could also be adjusted by changing the distributed distance of holes.

Fabrication of SI-TENG Device: For the SI-TENG, silicone rubber was chosen as the elastomeric dielectric. The liquid silicone rubber solution was prepared by mixing its two components in a 1:1 weight ratio (Ecoflex supersoft silicone 0050, Smooth-On, Inc.), then blended, and degassed in a vacuum for ≈ 5 min to thoroughly remove bubbles. The aforementioned acrylic plate with a conductive yarn network was surrounded by foam tape to prevent the liquid from flowing out. The liquid silicone rubber was then poured into the acrylic mold. The thickness of the SI-TENG could be adjusted based on the amount of silicone rubber. After curing in room temperature for ≈ 4 h, the elastomer film with the yarn network was removed from the acrylic plate. The residual silicone rubber remaining in the holes was removed with tweezers. Then, the elastomer film with yarn network was reversed, placed on an acrylic plate without holes, and immersed with liquid silicone rubber solution again. Under vacuuming, the surface of the elastomer film was covered by another acrylic plate with the same size as the bottom one. A certain amount of pressure was applied on the top acrylic plate to squeeze out the residual bubbles and the superfluous silicone rubber, as well as to make the device surface smooth. After curing, the SI-TENG with zigzag yarn conductive network was obtained.

Fabrication of Pressure Sensing Array: The SI-TENG-based pressure sensing array with 8×8 sensing units was fabricated with a similar method as the aforementioned SI-TENG. First, eight mutually independent conducting yarns were fixed on the bottom as the row layer, which were then covered by the first silicone rubber layer. After curing, another eight mutually independent conducting yarns were fixed on top along a perpendicular direction to the bottom yarns, constituting the column layer. Then, the above film was covered by the second silicone rubber layer. The solidified film was slowly removed from the acrylic plate. The following steps were the same as the above SI-TENG device. Finally, a stretchable and conformable SI-TENG-based pressure sensing array was obtained.

Washing Test: The experimental simulated washing environment was first cultivated in a beaker with household detergent and a magnetic stir bar added. Then, an SI-TENG device was directly put into the washing solution without any packaging. Afterward, the as-prepared beaker was placed on a magnetic stirrer to imitate agitator rotation in a household washing machine. The spinning speed of the magnetic stirrer was set at 600 rpm, and one washing cycle lasted for 20 min. Finally, the SI-TENG was rapidly dried in an oven at 60°C for later electrical output measurement.

Device Characterizations: The surface morphology of the three-ply-twisted silver-coated nylon yarn was characterized by field emission scanning electron microscopy (SU-8010, Hitachi). A commercial linear mechanical motor (LinMot E1100) was applied to mimic human motions, providing the periodic contact separation movement for the SI-TENG. A compression dynamometer (Vernier LabQuest Mini) was used to measure the applied force. The OC voltage (V_{OC}), SC current (I_{SC}), and SC charge transfer (Q_{SC}) were measured by an electrometer (Keithley, model 6541). The mechanical tensile test was conducted by a universal materials tester (MTS, Model Insight 10). The diameter was measured by an electronic digital micrometer (733 Series Electronic Digital Micrometers, L. S. Starrett).

Supporting Information

Supporting Information is available from the Wiley Online Library or from the author.

Acknowledgements

K.D. and Z.W. contributed equally to this work. The authors are grateful for the support received from the “Thousands Talents” program for the pioneer researcher and his innovation team in China, the Presidential Funding of the Chinese Academy of Science and the National Natural Science Foundation of China (Grants Nos. 51432005, 5151101243,

51561145021, and 51702353), and Beijing Municipal Science & Technology Commission (Grant No. Z171100000317001). K.D. thanks the China Scholarship Council for supporting research at the Georgia Institute of Technology, USA and the Fundamental Research Funds for the Central Universities (Grant No. 2232018G-02), China. K.D. and Z.L.W. are the inventors on the patent application (No.201810879626.2). No formal approval for the experiments involving human volunteers was required. The volunteers took part following informed consent.

Conflict of Interest

The authors declare no conflict of interest.

Keywords

electronic skin, energy harvesting, human–machine interfaces, pressure sensing, triboelectric nanogenerators

Received: July 31, 2018

Published online:

- [1] B. C. Tee, C. Wang, R. Allen, Z. Bao, *Nat. Nanotechnol.* **2012**, *7*, 825.
- [2] C. Larson, B. Peele, S. Li, S. Robinson, M. Totaro, L. Beccai, B. Mazzolai, R. Shepherd, *Science* **2016**, *351*, 1071.
- [3] X. Pu, M. Liu, X. Chen, J. Sun, C. Du, Y. Zhang, J. Zhai, W. Hu, Z. L. Wang, *Sci. Adv.* **2017**, *3*, e1700015.
- [4] Q. Hua, J. Sun, H. Liu, R. Bao, R. Yu, J. Zhai, C. Pan, Z. L. Wang, *Nat. Commun.* **2018**, *9*, 244.
- [5] Y. C. Lai, J. Deng, S. Niu, W. Peng, C. Wu, R. Liu, Z. Wen, Z. L. Wang, *Adv. Mater.* **2016**, *28*, 10024.
- [6] C. Pan, L. Dong, G. Zhu, S. Niu, R. Yu, Q. Yang, Y. Liu, Z. L. Wang, *Nat. Photonics* **2013**, *7*, 752.
- [7] W. Wu, X. Wen, Z. L. Wang, *Science* **2013**, *340*, 952.
- [8] T. Q. Trung, N. E. Lee, *Adv. Mater.* **2016**, *28*, 4338.
- [9] X. Wang, Y. Gu, Z. Xiong, Z. Cui, T. Zhang, *Adv. Mater.* **2014**, *26*, 1336.
- [10] G. Schwartz, B. C. Tee, J. Mei, A. L. Appleton, D. H. Kim, H. Wang, Z. Bao, *Nat. Commun.* **2013**, *4*, 1859.
- [11] C. Wang, D. Hwang, Z. Yu, K. Takei, J. Park, T. Chen, B. Ma, A. Javey, *Nat. Mater.* **2013**, *12*, 899.
- [12] J. Ge, L. Sun, F. R. Zhang, Y. Zhang, L. A. Shi, H. Y. Zhao, H. W. Zhu, H. L. Jiang, S. H. Yu, *Adv. Mater.* **2016**, *28*, 722.
- [13] T. Someya, T. Sekitani, S. Iba, Y. Kato, H. Kawaguchi, T. Sakurai, *Proc. Natl. Acad. Sci. USA* **2004**, *101*, 9966.
- [14] Z. Lou, L. Li, L. Wang, G. Shen, *Small* **2017**, *13*, 1701791.
- [15] S. Bauer, S. Bauer-Gogonea, I. Graz, M. Kaltenbrunner, C. Keplinger, R. Schwoiauer, *Adv. Mater.* **2014**, *26*, 149.
- [16] M. L. Hammock, A. Chortos, B. C. Tee, J. B. Tok, Z. Bao, *Adv. Mater.* **2013**, *25*, 5997.
- [17] X. Wang, L. Dong, H. Zhang, R. Yu, C. Pan, Z. L. Wang, *Adv. Sci.* **2015**, *2*, 1500169.
- [18] Q. Sun, W. Seung, B. J. Kim, S. Seo, S. W. Kim, J. H. Cho, *Adv. Mater.* **2015**, *27*, 3411.
- [19] N. T. Tien, S. Jeon, D. I. Kim, T. Q. Trung, M. Jang, B. U. Hwang, K. E. Byun, J. Bae, E. Lee, J. B. Tok, Z. Bao, N. E. Lee, J. J. Park, *Adv. Mater.* **2014**, *26*, 796.
- [20] S. Park, H. Kim, M. Vosgueritchian, S. Cheon, H. Kim, J. H. Koo, T. R. Kim, S. Lee, G. Schwartz, H. Chang, Z. Bao, *Adv. Mater.* **2014**, *26*, 7324.
- [21] Y. Ai, Z. Lou, S. Chen, D. Chen, Z. M. Wang, K. Jiang, G. Shen, *Nano Energy* **2017**, *35*, 121.

- [22] Z. Lou, S. Chen, L. Wang, R. Shi, L. Li, K. Jiang, D. Chen, G. Shen, *Nano Energy* **2017**, *38*, 28.
- [23] B. Zhu, Z. Niu, H. Wang, W. R. Leow, H. Wang, Y. Li, L. Zheng, J. Wei, F. Huo, X. Chen, *Small* **2014**, *10*, 3625.
- [24] L. Pan, A. Chortos, G. Yu, Y. Wang, S. Isaacson, R. Allen, Y. Shi, R. Dauskardt, Z. Bao, *Nat. Commun.* **2014**, *5*, 3002.
- [25] U. Khan, T. H. Kim, H. Ryu, W. Seung, S. W. Kim, *Adv. Mater.* **2017**, *29*.
- [26] G. Zhu, W. Q. Yang, T. Zhang, Q. Jing, J. Chen, Y. S. Zhou, P. Bai, Z. L. Wang, *Nano Lett.* **2014**, *14*, 3208.
- [27] Z. L. Wang, *ACS Nano* **2013**, *7*, 9533.
- [28] Z. L. Wang, *Faraday Discuss.* **2014**, *176*, 447.
- [29] Z. L. Wang, J. Chen, L. Lin, *Energy Environ. Sci.* **2015**, *8*, 2250.
- [30] Z. L. Wang, L. Lin, J. Chen, S. Niu, Y. Zi, *Triboelectric Nanogenerators*, Springer International Publishing, Berlin, Germany **2016**.
- [31] Z. L. Wang, *Adv. Mater.* **2012**, *24*, 280.
- [32] K. Dong, J. Deng, Y. Zi, Y. C. Wang, C. Xu, H. Zou, W. Ding, Y. Dai, B. Gu, B. Sun, Z. L. Wang, *Adv. Mater.* **2017**, *29*, 1702648.
- [33] K. Dong, Y.-C. Wang, J. Deng, Y. Dai, S. L. Zhang, H. Zou, B. Gu, B. Sun, Z. L. Wang, *ACS Nano* **2017**, *11*, 9490.
- [34] P. Wang, R. Liu, W. Ding, P. Zhang, L. Pan, G. Dai, H. Zou, K. Dong, C. Xu, Z. L. Wang, *Adv. Funct. Mater.* **2018**, 1705808.
- [35] S. Wang, L. Lin, Z. L. Wang, *Nano Energy* **2015**, *11*, 436.
- [36] J. Chen, Z. L. Wang, *Joule* **2017**, *1*, 480.
- [37] K. Dong, J. Deng, W. Ding, A. C. Wang, P. Wang, C. Cheng, Y.-C. Wang, L. Jin, B. Gu, B. Sun, Z. L. Wang, *Adv. Energy Mater.* **2018**, *8*, 1801114.
- [38] D. A. Davis, A. Hamilton, J. Yang, L. D. Cremer, D. Van Gough, S. L. Potisek, M. T. Ong, P. V. Braun, T. J. Martinez, S. R. White, J. S. Moore, N. R. Sottos, *Nature* **2009**, *459*, 68.
- [39] S. L. Potisek, D. A. Davis, N. R. Sottos, S. R. White, J. S. Moore, *J. Am. Chem. Soc.* **2007**, *129*, 13808.
- [40] G. O'Bryan, B. M. Wong, J. R. McElhanon, *ACS Appl. Mater. Interfaces* **2010**, *2*, 1594.
- [41] C. Jacquemoud, K. Bruyeregarnier, M. Coret, *J. Biomech.* **2007**, *40*, 468.
- [42] S. Niu, Y. Liu, S. Wang, L. Lin, Y. S. Zhou, Y. Hu, Z. L. Wang, *Adv. Funct. Mater.* **2014**, *24*, 3332.
- [43] M. F. O'Rourke, *Am. Heart J.* **1971**, *82*, 687.
- [44] M. F. O'Rourke, R. P. Kelly, *J. Hypertens.* **1993**, *11*, 327.